

1 **Organic coating on sulfate and soot particles during late summer in**
2 **the Svalbard Archipelago**

3

4 Hua Yu^{1,2}, Weijun Li^{2*}, Yangmei Zhang³, Peter Tunved⁴, Manuel Dall'Osto⁵, Xiaojing
5 Shen³, Junying Sun³, Xiaoye Zhang³, Jianchao Zhang⁶, Zongbo Shi^{7,8*}

6

7 ¹Key Laboratory of Hangzhou City for Ecosystem Protection and Restoration, College of Life and
8 Environmental Sciences, Hangzhou Normal University, Hangzhou, 310036, China

9 ²Department of Atmospheric Sciences, School of Earth Sciences, Zhejiang University, 310027,
10 Hangzhou, China

11 ³Key Laboratory of Atmospheric Chemistry, Chinese Academy of Meteorological Sciences, Beijing,
12 China

13 ⁴Department of Environmental Science and Analytical Chemistry, Stockholm University, 10691,
14 Stockholm, Sweden

15 ⁵Institute of Marine Sciences, ICM-CSIC, Passeig Marí de la Barceloneta, 37-49, E-08003,
16 Barcelona, Spain

17 ⁶Key Laboratory of the Earth's Deep Interior, Institute of Geology and Geophysics, Chinese Academy
18 of Sciences, 100029, China

19 ⁷School of Geography, Earth and Environmental Sciences, the University of Birmingham, Birmingham,
20 UK

21 ⁸Institute of Surface Earth System Science, Tianjin University, Tianjin, China

22

23 *Corresponding Emails: liweijun@zju.edu.cn; z.shi@bham.ac.uk

24

25 **Abstract**

26 Interaction of anthropogenic particles with radiation and clouds plays an important
27 role on Arctic climate change. Mixing state of aerosols is a key parameter to influence
28 aerosol radiation and aerosol-cloud interaction. However, little is known on this
29 parameter in the Arctic, preventing an accurate representation of this information in
30 global models. Here we used transmission electron microscopy with
31 energy-dispersive X-ray spectrometry, scanning electron microscopy, nanoscale
32 secondary ion mass spectrometry, and atomic forces microscopy to determine the size
33 and mixing state of individual sulfate and carbonaceous particles at 100 nm – 2 μ m
34 collected in the Svalbard Archipelago in summer. We found that 74% by number of
35 non-sea salt sulfate particles were coated with organic matter (OM). 20% of sulfate
36 particles also had soot inclusions which only appeared in the OM coating. The OM
37 coating is estimated to contribute to 63% of the particle volume on average. To
38 understand how OM coating influences optical properties of sulfate particles, a Mie
39 core-shell model was applied to calculate optical properties of individual sulfate
40 particles. Our result shows that absorption cross section of individual OM-coated
41 particles significantly increased when assuming the OM coating as light-absorbing
42 brown carbon. Microscopic observations here suggest that OM modulates the mixing
43 structure of fine Arctic sulfate particles, which may determine their hygroscopicity
44 and optical properties.

45

46 **1. Introduction**

47 Surface temperatures are rising faster in the Arctic than the rest of globe (IPCC,
48 2013). Although increased human-induced emissions of long-lived greenhouse gases
49 are certainly one of the driving factors, air pollutants, such as aerosols and ozone, are
50 also important contributors to climate change in the Arctic (Law and Stohl, 2007;
51 Shindell, 2007). Spatial and temporal variations of aerosol composition, size
52 distribution, and sources of Arctic aerosols have been studied extensively in numerous
53 ground-based, ship, airborne observations, and various atmospheric models (Brock et
54 al., 2011; Burkart et al., 2017; Chang et al., 2011; Dall'Osto et al., 2017; Fu et al.,
55 2008; Hara et al., 2003; Hegg et al., 2010; Iziomon et al., 2006; Karl et al., 2013;
56 Latham et al., 2013; Leck and Bigg, 2008; Leck and Svensson, 2015; Moore et al.,
57 2011; Raatikainen et al., 2015; Wörnschimmel et al., 2013; Winiger et al., 2017;
58 Yang et al., 2018; Zangrando et al., 2013). These studies show that regional pollutants
59 and local natural aerosol production affect sea ice albedo and the heat balance of the
60 atmosphere, especially in the summer when mid-latitude transport is not as frequent
61 relative to that during the winter/spring Arctic Haze season (Hansen and Nazarenko,
62 2004; Jacob et al., 2010; Shindell, 2007).

63 Aerosol particles in the Arctic atmosphere are mainly composed of sea salt, sulfate,
64 particulate organic matter (OM) with a small amount of ammonium, nitrate, black
65 carbon (BC) (Hara et al., 2003; Quinn et al., 2007) and mineral dust particles
66 (Dagsson-Waldhauserova et al., 2013). Sea salts, derived from the Arctic Ocean, are
67 the dominant coarse particles ($>1 \mu\text{m}$) in the Arctic atmosphere (Behrenfeldt et al.,
68 2008; Chi et al., 2015). Compared to other types of aerosols, sea salt is the largest
69 contributor to radiative forcing in remote Ocean air (Wang et al., 2019). Natural sea
70 salt particles can provide large surfaces for heterogeneous reaction with acidic gases
71 in the Arctic air (Chi et al., 2015; Geng et al., 2010; Hara et al., 2003). Moreover, sea
72 salt particles are an important source of cloud condensation nucleation (CCN) in the
73 Arctic air (Abbatt et al., 2019); Coarse dust particles in the Svalbard region have been
74 observed to be occasionally influenced from local (Svalbard) and/or distant (e.g.,
75 Iceland, Greenland and Siberia) sources in high latitudes (Behrenfeldt et al., 2008).

76 Tobo et al. (2019) showed that glacial outwash sediments in Svalbard (a proxy for
77 glacially sourced dusts) due to the recent rapid and widespread retreat of glaciers have
78 a remarkably high ice nucleating ability under conditions relevant for mixed-phase
79 cloud formation.

80 BC, commonly called “soot”, is derived from the combustion sources such as
81 diesel engines, residential solid fuel, and open burning (Bond et al., 2013). Studies
82 show BC in the Arctic absorbs solar radiation in the atmosphere and when deposited
83 on snow (Iziomon et al., 2006; Koch and Hansen, 2005; Sand et al., 2013; Shindell,
84 2007). Maahn et al. (2017) found that BC concentration is enhanced below the clouds
85 in the Arctic. This influences the mean effective radii of cloud droplets which lead to
86 the suppressed drizzle production and precipitation. Possible sources of BC particles
87 in the Arctic include natural gas flaring (Qi et al., 2017), ship emissions (Browse et al.,
88 2013; Weinbruch et al., 2012) and long range transport from emissions of biomass
89 burning and fossil fuels in the northern hemisphere (Winiger et al., 2016; Xu et al.,
90 2017). Winiger et al.(2017) showed that most of the Arctic BC is from domestic
91 activities (35%) and transportation (38%), with only minor contributions from gas
92 flaring (6%), power plants (9%), and open fires (12%).

93 OM is a significant component in Arctic aerosol (Quinn et al., 2007). More than
94 100 organic species have been detected in the Arctic aerosols and polyacids are the
95 most abundant compound class, followed by phthalates, aromatic acids, fatty acids,
96 fatty alcohols, sugars/sugar alcohols, and n-alkanes (Fu et al., 2008). Recently, certain
97 organic aerosols, referred to as brown carbon (BrC), have been recognized as an
98 important light-absorbing carbonaceous aerosol in the troposphere (Alexander et al.,
99 2008; Andreae and Gelencser, 2006; Feng et al., 2013; Lack et al., 2012). BrC can be
100 directly emitted from combustion sources or form in the atmosphere via
101 photo-chemical aging (Jiang et al., 2019; Saleh et al., 2013; Updyke et al., 2012).
102 Moreover, aging of secondary organic aerosols can significantly contribute to BrC
103 during atmospheric transport (Laskin et al., 2015). Feng et al.(2013) estimated that on
104 average, BrC accounts for 66% of total OM mass globally and its light absorption is
105 about 26% of BC.

106 Sulfate is a dominant aerosol component in the Arctic air (Quinn et al., 2007). The
107 Community Earth System Model simulations show that sources from East Asia have
108 the largest contribution to the Arctic sulfate column burden, with an annual mean
109 contribution of 27%, followed by 11–13% each from South Asia, the rest of the world
110 (including the Arctic), and Russia/Belarus/Ukraine sources and 13% from natural
111 sources (Yang et al., 2018). Large amounts of secondary species including sulfate and
112 OM not only change radiative forcing and number of CCN in Arctic atmosphere
113 (Abbatt et al., 2019; Yang et al., 2018) but also influence optical, hygroscopic, and
114 CCN activity of these internally mixed BC and mineral dust particles (Latham et al.,
115 2013; Raatikainen et al., 2015; Zanatta et al., 2018).

116 BC and BrC are often internally mixed with other non-absorbing aerosols, such as
117 sulfate (Lack et al., 2012; Laskin et al., 2015). Internal mixing means that a single
118 particle simultaneously contains two or more types of aerosol components (Li et al.,
119 2016). This internal mixing can enhance BC absorption by a factor of two (Bond et al.,
120 2013) and change the activity of CCN in the Arctic atmosphere (Leck and Svensson,
121 2015; Martin et al., 2011). A few previous studies also looked at the mixing states of
122 coarse aerosol particles in Arctic troposphere (Behrenfeldt et al., 2008; Chi et al.,
123 2015; Geng et al., 2010; Hara et al., 2003; Leck and Svensson, 2015; Moroni et al.,
124 2017; Raatikainen et al., 2015; Sierau et al., 2014), but those of fine non-sea salt
125 particles, including the most important short-lived climate forcers – BC and BrC
126 (Feng et al., 2013; Fu et al., 2008; Kirpes et al., 2018; Laskin et al., 2015; Leck and
127 Svensson, 2015), are poorly characterized. A poor understanding on mixing state of
128 BC and BrC in individual particles prevents an accumulate simulation of the direct
129 aerosol forcing and aerosol-cloud interaction in the Arctic (Browse et al., 2013;
130 Samset et al., 2014; Zanatta et al., 2018).

131 In this study, individual aerosol particles were collected in Svalbard during 7-23
132 August, 2012. We combined the data from various microscopic instruments to
133 determine the size, composition, and mixing properties of individual particles, with a
134 particular focus on sulfate and carbonaceous particles. Mie theory was used to test
135 how OM coating influences optical properties of sulfate particles in the Arctic when

136 OM was assumed as BrC. The results are discussed in the context of aerosol radiation
137 and aerosol-cloud interaction.

138

139 **2. Experimental section**

140 **2.1 Field campaign**

141 The Svalbard archipelago includes all landmasses between 74 and 81 degrees
142 North and 10 and 35 degrees East (Figure 1). The islands cover 63000 km².
143 Ny-Ålesund town is situated on the west coast of the largest island, Spitsbergen and
144 1200 km from the North Pole. It is a central platform for Arctic research.

145 The observation site is based at the Chinese Arctic Yellow River Station (78°55'N,
146 11°56'E) (Chi et al., 2015; Geng et al., 2010). The site is about 2 km far away from
147 the Zeppelin observatory station (78.9N 11.88E) run by the Ny-Ålesund Science
148 Managers Committee. On the west coast of the island of Spitsbergen, Ny-Ålesund is a
149 Norwegian research and monitoring infrastructure, hosting national and international
150 research projects and programmes. The Norwegian Polar Institute (NPI) runs the
151 Sverdrup Research Station at the coast and Zeppelin Observatory at the Mountain 475
152 m asl, and Sweden, Germany, France, Italy, Japan, China, England, The Netherlands,
153 South Korea, and India are the other countries to have established long-term
154 programmes in Ny-Ålesund (<https://www.esrl.noaa.gov/psd/iasoa/stations/nyalesund>).
155 Two to three samples were regularly collected at 9:00, 16:00, 21:00 (local time) of
156 each day, with a total of 46 samples during 7-23 August, 2012.

157 A sampler containing a single-stage impactor with a 0.5-mm-diameter jet nozzle
158 (Genstar Electronic Technology, China) was used to collect individual particles by the
159 air flow rate at 1.5 l min⁻¹. Aerosol particles were collected onto copper TEM grids
160 coated with carbon film. This sampler has a collection efficiency of 31% at 100 nm
161 aerodynamic diameter and 50% at 200 nm assuming the density of the particles is 2 g
162 cm⁻³. Sampling times varied from twenty minutes to two hours depending on the
163 loading of particles. After collection, each sample was placed in a sealed dry plastic
164 tube and stored in a desiccator at 20 ± 3% RH for analysis. Ambient laboratory
165 conditions (17–23% RH and 19–21 °C) is effective at preserving individual

166 hygroscopic aerosol particles and reducing changes that would alter samples and
167 subsequent data interpretation (Laskina et al., 2015). During the sampling period,
168 meteorological data at the sampling site including pressure (P), relative humidity
169 (RH), temperature (T), wind speed (WS), and wind direction (WD) were recorded
170 every 5 min using a pocket weather meter (Kestrel 4500, Nielsen-Kellermann Inc.,
171 USA). Sample information including local sampling date and time and various
172 meteorological conditions are listed in Table 1.

173

174 **2.2 TEM measurement**

175 Individual particle samples were examined by a JEOL JEM-2100 transmission
176 electron microscopy operated at 200 kV with an energy-dispersive X-ray
177 spectrometry (TEM/EDS). TEM can observe the mixing structure of different aerosol
178 components within an individual particle on the substrate because electron beam
179 transmit through the specimen to form an image. EDS spectra are acquired for a
180 maximum time of 30 s to minimize potential beam damage and collect particle X-ray
181 spectra with sufficient intensity. TEM grids are made of copper (Cu) and covered by a
182 carbon-reinforced substrate, so Cu is excluded from the quantitative analyses of the
183 particles. Because of the substrate contribution, C content in TEM grid coated by
184 carbon film might be overestimated in EDS spectra of individual particles.

185 The distribution of aerosol particles on TEM grids was not uniform, with coarser
186 particles occurring near the center and finer particles on the periphery. Therefore, to
187 ensure that the analysed particles are representative, five areas were chosen from the
188 center to periphery of the sampling spot on each grid. Through a labor-intensive
189 operation, 2002 aerosol particles with diameter < 10 μm in 21 samples were analysed
190 by TEM/EDS (Table 1). To check elemental composition of individual particles, EDS
191 was manually used to obtain elemental spectra of individual particles. In the clean
192 Arctic air, there are simple particle types including sea salt, sulfate, soot, OM, and
193 mineral. Because soot particles have chain-like aggregation, it is not necessary to
194 check their elemental composition. Sea salt particles display spherical or square
195 shapes and are stable under the electron beam in TEM (Chi et al., 2015). Sulfate

196 particles are spherical but flats on the substrate and produce unstable bubble under the
197 electron beam (Buseck and Posfai, 1999). TEM observations can also identify sulfate
198 particles or sulfate with OM coating. TEM/EDS analysis is very time-consuming.
199 Thus, we did not check the composition of every single particle analysed. Instead, we
200 randomly checked the elemental composition of 20-30 particles in each sample (Table
201 1). EDS spectra of 575 particles were manually selected and saved in the computer for
202 elemental composition analysis. Particles examined by TEM were dry at the time of
203 observation in the vacuum of the electron microscope. In our study, the effects of
204 water and other semi-volatile organics were not considered as they evaporated in the
205 vacuum.

206 Elemental mapping and line profile of selected individual aerosol particles were
207 also obtained from the EDS scanning operation mode of TEM (STEM). The STEM
208 information clearly display elemental distribution in the targeted individual particles
209 which cannot be provided by the above EDS analysis. Based on preliminary
210 individual analysis, we further chose the typical samples containing abundant sulfate
211 with OM coating for the STEM analysis. High-resolution elemental distribution in
212 individual particles provides detailed mixing structure of sulfate and OM in individual
213 particles.

214 The iTEM software (Olympus soft imaging solutions GmbH, Germany) is an
215 image analysis platform for electron microscopy. In this study, it was used to
216 manually or automatically obtain area, perimeter, and equivalent circle diameter
217 (ECD) of individual particles. In these analysed samples, we found there were
218 abundant sulfate particles (~30% by number) in the 11 samples collected during 9-15
219 August, 2012. In other samples, there are more sea salt particles with few particles.
220 Based on the TEM observations, we selected the samples containing more sulfate
221 particles for further microscopic analyses (see below).

222

223 **2.3 NanoSIMS measurement**

224 Because the sulfate particles in different samples collected in the Arctic had
225 similar elemental composition and mixing state from the TEM observations, we

226 selected three samples (Table 1) for nanoscale secondary ion mass spectrometry
227 (NanoSIMS) analysis (CAMECA Instruments, Geneviers, France). A micro-caesium
228 source was used to generate Cs⁺ primary ions, with an impact energy of 16 kV for
229 sample interrogation. The primary beam was stepped across the sample to produce
230 element specific, quantitative digital images. The Cs⁺ primary ion beam was used to
231 obtain ¹⁶O⁻, ¹²C¹⁴N⁻, ¹⁴N¹⁶O⁻, ³²S⁻, ³⁵Cl⁻, and ¹⁶O²³Na⁻ ions in this study. The
232 NanoSIMS analysis can obtain ion mapping of particles with nanometer spatial
233 resolution over a broad range of particle sizes (Figure S1). Because the substrate of
234 TEM grid is carbon, CN⁻ is adopted to represent OM in individual particles (Chi et al.,
235 2015; Ghosal et al., 2014). S⁻ is used to infer the presence of sulfates in individual
236 particles (Li et al., 2017). A total of 32 sulfate containing particles were analysed by
237 the NanoSIMS.

238

239 **2.4 SEM measurement**

240 We used a Zeiss ultra 55 scanning electron microscopy (SEM) with EDS to
241 examine the vertical distribution of OM and sulfate in individual particles. TEM grids
242 were mounted onto an aluminum SEM stub and directly observed in secondary
243 electron image mode. SEM analysis was operated at 10 kv of extra high tension (EHT)
244 and 9.7 mm of work distance (WD). Processes such as sample moving, analysis
245 region selection and imaging were controlled by computer. The specimen stage in
246 SEM was tilted at the range of 0-75°, and then we vertically observed thickness of
247 OM coating and sulfate core on the substrate. Two typical samples that contain
248 abundant sulfate particles were chosen for this analysis (Table 1).

249 **2.5 AFM measurement**

250 AFM with a digital nanoscope IIIa instrument operating in the tapping mode was
251 used to observe surface morphology of individual aerosol particles and measure
252 particle thickness. The tapping AFM has a cantilever and conical tip of 10 nm radius.
253 By using AFM, a general image of the particles is taken at 10 μm full scan size, which
254 generally includes 1-2 particles depending on the exact location. In this study, we are
255 only interested in the sulfate-containing particles. AFM provides surface information

256 and morphology of 17 particles but no composition. Samples were firstly quickly
257 examined by the TEM under low magnification mode to find sulfate-containing
258 particles. Because TEM grids have coordinates letters, we can find the same
259 particles in the AFM. This analysis provides 3-D image of the sulfate-containing
260 particles and their volume. After we obtained AFM images of sulfate particles, the
261 NanoScope analysis software can automatically obtain bearing area (A) and bearing
262 volume (V). This can then be converted into equivalent circle diameter (d, ECD) and
263 equivalent spherical diameter (D, ESD)

$$264 \quad A = \frac{4}{3} \pi r^2 = \frac{\pi d^2}{3} \rightarrow d = \sqrt{\frac{3A}{\pi}} \quad (1)$$

$$265 \quad V = \frac{4}{3} \pi r^3 = \frac{4}{3} \times \frac{\pi D^3}{8} \rightarrow D = \sqrt[3]{\frac{6V}{\pi}} \quad (2)$$

266 ESD and ECD of sulfate-containing particles are well corrected. Using the linear
267 correlation equation (ESD=0.38ECD), we can then correct the ESD of individual
268 particles from TEM analysis to obtain the ECD (Chi et al., 2015).

269

270 **2.6 Calculation of BrC optical properties**

271 The refractive index used for the non-light-absorbing sulfate component was set to
272 $m=1.55$ at 550 nm (Seinfeld and Pandis, 2006). The refractive index of OM (as BrC)
273 is not known so we considered three scenarios: strongly absorbing ($1.65-0.03i$ at 550
274 nm), moderately absorbing ($1.65-0.003i$ at 550 nm), and non-absorbing OM (1.65 at
275 550 nm) (Feng et al., 2013). Here, we choose 550 nm as a case study to test how OM
276 coating influence sulfate particles in Arctic air.

277 BHCOAT Mie code by Bohren and Huffman (1983) was used to calculate the
278 optical properties, including scattering cross section (SCS), absorption cross section
279 (ACS), and single scattering albedo (SSA), assuming a core-shell structure. We firstly
280 calculated these parameters assuming a sulfate core and OM shell structure only
281 (ignoring some of the particles that contain soot core). Because the Mie code only can
282 calculate the core-shell structure or homogeneous model, we assume sulfate as a core
283 and OM as a shell in individual particle to build the core-shell model. Based on the

284 core-shell standard mode (Li et al., 2016), we can calculate optical properties of
285 individual internally mixed particles.

286 **2.7 Back trajectories of air masses and Lagrangian particle dispersion model**

287 Three-day (72 h) back trajectories of air masses were generated using a Hybrid
288 Single Particle Lagrangian Integrated Trajectory (HYSPLIT) model at the Chinese
289 Arctic Yellow River Station during August 2012. Here we selected an altitude of 500
290 m as the end point in each back trajectory (Figure 1). Back trajectories for 50 m and
291 1000 m above sea level are similar.

292 A lagrangian particle dispersion model FLEXPART-WRF 3.1 (Brioude et al.,
293 2013) was also used to examine the origin of particles. The FLEXPART-WRF model
294 is using meteorological parameters from WRF dynamical simulation. The domain
295 resolution is 50×50 km with 64 vertical levels. The FLEXPART-WRF simulations
296 were launched in a backward mode over 10 days, with the Chinese Arctic Yellow
297 River Station as an origin. For each simulation (one per sample), 20000
298 pseudo-particles were released in a small volume around the station position. Each
299 single particle position evolution backward in time was determined by Lagrangian
300 dispersion calculation.

301 Based on the TEM experiments and back trajectory of air masses (Figure 1), we
302 found that there were more S-rich with OM coating particles in the samples collected
303 on August 11, 12, 14, and 15, 2012. Therefore, we further did the FLEXPART-WRF
304 simulation of these four days (Figure 2). The emission intensity in the Arctic area has
305 been also shown in Figure S2.

306 **3. Results**

307 **3.1 Composition and source of aerosol particles**

308 TEM/EDS analysis shows that O, Na, S, and Cl are dominant elements in
309 individual particles (Figure S3). On basis of the composition and morphology of
310 individual particles, we classified the particles into four major groups: Na-rich (i.e.
311 NaCl, Na₂SO₄, and NaNO₃), S-rich (i.e. ammonium sulfate and sulfuric acid),
312 carbonaceous (soot and OM), and mineral dust particles. The classification criteria of
313 different particle types and their sources have been described in a separate study (Li et

314 al., 2016). S-rich particles representing secondary inorganic particles (e.g., SO_4^{2-} ,
315 NO_3^- , and NH_4^+) are converted from gaseous SO_2 , NO_x , and NH_3 . OM can be divided
316 into primary organic matter (POM) and secondary organic matter (SOM). SOM is
317 produced from the chemical oxidation of volatile organic compounds (VOCs) and
318 often exhibits OM coating on S-rich particles (Li et al., 2016; Moffet et al., 2013;
319 Riemer et al., 2019). Na-rich particles in the marine air are from sea spray and have
320 typical near cubic shape. Mineral dust particles from natural ground soil contain Si, Al,
321 or Ca and have irregular shape. Soot particles, which contain C with minor O, appear
322 as a chain-like aggregate of carbon-bearing spheres. Chi et al. (2015) studied the
323 aging mechanism of sea salt particles. Here, we focused on non-sea salt (NSS)
324 particles including S-rich, soot, and OM particles NSS-particles and
325 sulfate-containing particles account for $39 \pm 5\%$ and $29 \pm 7\%$ by number of all the 2002
326 particles analysed (Figure 3).

327

328 **3.2 OM coating on sulfate particles**

329 TEM observations revealed a common core-shell mixing structure in fine
330 sulfate-containing particles (Figure 4a). Elemental mapping of such internally mixed
331 sulfate particles shows C signals in the coating (C map, Figure 4b) and S and O
332 signals in the center (S and O map, Figure 4c, d). The elemental line profile of a
333 sulfate particle also shows sulfate core and C coating (Figure S4). Furthermore, ion
334 maps of individual particles from the NanoSIMS further show $^{12}\text{C}^{14}\text{N}$ signals in the
335 coating (red color in Figure 4e, f) and ^{32}S signals in the core (green color in Figure 4e,
336 g). These results provide strong evidence that the coating is OM and the core is
337 sulfate.

338 A majority of the 781 analysed NSS-particles (74% by particle number) have a
339 sulfate core and OM coating (Figures 4 and 5). ~20% of them also contain small soot
340 inclusions but they only appeared in organic coating, rather than as the core (Figure
341 5b). The mixing structure is different from our previous findings in polluted air where
342 soot is normally mixed with sulfate instead of OM coating (Li et al., 2016). Moreover,
343 we observed some chain-like soot aggregates (1.3% in all analysed particles) (Figure

344 S5) but they only occurred in three samples during the whole sampling period (Table
345 1). Considering the remoteness of the sampling site, such fresh soot particles are
346 likely to be of local origin, for example, shipping and flaring (Gilgen et al., 2018;
347 Peters et al., 2011).

348 TEM observations showed that some sulfate-containing particles had unique
349 morphology that a sulfate particle was surrounded by some smaller particles (Figure
350 5a). They are often called “satellite” particles as they were distributed from the central
351 particles when impacted on the substrate during sample collection. Satellite particles
352 were observed around 16% of the analysed sulfate-containing particles (Figure 5a) in
353 the samples (Table 1) collected during 9-15 August. NanoSIMS analysis further
354 showed that the satellite particles (Table 1) have strong $^{32}\text{S}^-$ (Figure 6a, c) and $^{16}\text{O}^-$
355 signals (Figure 6d) as well as weak $^{12}\text{C}^{14}\text{N}^-$ signals (Figure 6a, b). Previous studies
356 showed that the similar satellite particles are normally considered as acidic sulfate
357 (Buseck and Posfai, 1999; Iwasaka et al., 1983). Our results show that these acidic
358 satellites not only contain sulfuric acid but also some OM or organic acids. Indeed, Fu
359 et al. (2008) found that polyacids are the most abundant organic compounds, followed
360 by phthalates, aromatic acids, and fatty acids in Arctic aerosol particles. Based on the
361 back trajectories of air masses and FLEXPART modelling, most air masses originate
362 in the North America and Greenland during the sampling periods (Figures 1 and 2).
363 Figure 1 shows that these air masses brought abundant sulfate-containing particles
364 into the sampling area in summertime.

365 AFM was used to obtain 3D image of individual secondary particles impacting on
366 the substrate. Figure 7a shows that the secondary particles normally have smooth
367 surface which is different from uneven surface of the Arctic fresh and aged NaCl
368 particles (Chi et al., 2015). Furthermore, we observed particle thickness through
369 tilting the specimen stage up to 75° in SEM. Figure 7a-b both shows that the
370 secondary particles look like thin pancake sticking on the substrate. Furthermore, the
371 sections of two secondary particles in the AFM images shows that the highest heights
372 of particles are only 15% (green line) and 26% (red line) of the corresponding
373 horizontal diameter (Figure 7a). These results show that the shape of individual

374 particles was modified when they impacted on the substrate following the airflow.
375 Therefore, the measured ECDs of individual particles in TEM images are much larger
376 than the real particle diameter. To calibrate the particle diameter, we obtained volume
377 of dry particles on the substrate and then calculated their ESD in the AFM images
378 (Figure 7c). ESD distribution of the secondary Arctic particles displayed a peak at 340
379 nm, ranging from 100 nm to 2000 nm (Figure 7d). The core particles, as sulfate or
380 soot, had a peak at 240 nm and 120 nm, respectively (Figure 7d). It is estimated that
381 OM on average accounted for $63 \pm 23\%$ of the dry sulfate-containing particle volume.
382 Our result shows that the OM volume increases following the particle size increase
383 (Figure S6).

384

385 **4. Discussion**

386 **4.1 Mixing mechanism of organic, soot, and sulfate**

387 Lagrangian particle dispersion modeling using the FLEXPART-WRF 3.1 showed
388 that air masses arriving at the sampling site during our field measurement periods
389 were likely originated from the Greenland and North America (Figure 2). Previous
390 studies reported that air masses from North America or Greenland during the summer
391 contain higher concentration of black carbon, OM, and sulfate (Burkart et al., 2017;
392 Chang et al., 2011; Fu et al., 2008; Moore et al., 2011; Park et al., 2013). Indeed, there
393 is strong emission intensity of OC and SO₂ around the Arctic area from emission
394 simulation as shown in Figure S2. However, Weinbruch et al. (2012) observed soot
395 particles when cruise ships were present in the area around Ny-Ålesund town. It is
396 possible that minor soot particles are from the ship emissions and most of them are
397 transported from outside Arctic area in the free troposphere (Figure S2).

398 The sulfate core-OM shell structure observed in the Arctic summer atmosphere is
399 similar to those in the background or rural air in other places (Li et al., 2016; Moffet
400 et al., 2013). Based on the images from electron microscopies, we can infer that OM
401 coating thickness in the Arctic air was comparable with them in rural places but
402 higher than them in urban places. During the transports, organic coatings on sulfate
403 were considered as the SOM and their masses increase following particle aging and

404 growth (Li et al., 2016; Moffet et al., 2013; Sierau et al., 2014). Figures 1 and 2 show
405 that most of particles in the air masses are transported from North American. The
406 sulfate/OM particles with soot inclusions are probably formed in a similar way as
407 those found elsewhere (Li et al., 2016) – e.g., soot particles may have acted as nuclei
408 for secondary sulfate or organic uptake during their transports (Riemer et al., 2009).
409 Similarly, besides the OM coating in the Arctic particles, Leck and Svensson (2015)
410 found biogenic aerosols like gel-aggregate containing bacterium in ultrafine particles.
411 However, we did not find any gel-like particles in the samples because our sampler
412 had very low efficiency for ultrafine particles.

413 TEM images show that most of the internally mixed sulfate-containing particles
414 display sulfate core and OM coating on the substrate (Figures 4a and 5b, c).
415 Knowledge on the phase separation in individual particles is important to understand
416 particle hygroscopic properties, heterogeneous reactions of reactive gases on particle
417 surface, and organic aging (You et al., 2012). It is possible that the thick OM coatings
418 were consistently built up during the long-range transport of sulfate-containing
419 particles and part of the SOM in the coating likely formed in Arctic area. Indeed, there
420 are various sources of organic precursors during the Arctic area, such as biogenic
421 VOCs from ice melting and open water (Dall'Osto et al., 2017) and anthropogenic
422 VOCs from shipping emissions in summertime (Gilgen et al., 2018). The dependence
423 of OM volume on particle size (Figure S6) suggests that the suspended sulfate
424 particles are initially important surface for SOM formation. Moreover, the presence of
425 OM coating in 74% sulfate particles indicates that SOM as the surfaces of fine
426 particles may govern the possible heterogeneous reactions between reactive gases and
427 sulfate-containing particles in the Arctic air.

428 It should be noted that most of SOM not only occurred on the surfaces of
429 sulfate-containing particles but also its mass (mean mass at $63 \pm 23\%$) dominated in
430 individual particles (Figure 7d). The OM dominating in individual particles can
431 influence the IN and CCN activities of secondary sulfate-containing particles (Latham
432 et al., 2013; Martin et al., 2011). For example, some studies found that an increase in
433 organic mass fraction in particles of a certain size would lead to a suppression of the

434 Arctic CCN activity (Leck and Svensson, 2015; Martin et al., 2011). Moreover, OM
435 as particle surfaces can significantly influence hygroscopicity and IN activity of
436 sulfate-containing particles (Wang et al., 2012).

437

438 **4.2 Potential impact of OM on optical properties of sulfate-containing particles**

439 The internal mixing of soot, sulfate, and OM can change optical properties of
440 individual particles in the atmosphere. Recent studies showed that BrC has been
441 detected in the OM in the polluted and clean air and even in upper troposphere
442 (Laskin et al., 2015; Wang et al., 2018). Feng et al. (2013) further calculated the
443 contribution up to 19% of the optical absorption of the strongly absorbing BrC in
444 global simulations which is after the absorption BC aerosols. Various colored OM (e.g.
445 nitrated/polycyclic aromatics and phenols), referred as BrC, were detected in the
446 Arctic atmosphere in different seasons (Fu et al., 2008; Währnschimmel et al., 2013;
447 Zangrando et al., 2013) and in surface ice or snowpack (Browse et al., 2013; Doherty
448 et al., 2013; Hegg et al., 2010). We also noticed that the $^{12}\text{C}^{14}\text{N}^-$ signal occurred in all
449 analysed OM coating in sulfate-containing particles (Figure 4e-f). $^{12}\text{C}^{14}\text{N}^-$ from
450 NanoSIMS is indicative of the presence of nitrogen-containing organic in the detected
451 materials (Herrmann et al., 2007). Figure 4 showed that the nitrogen-containing OM
452 was more or less homogeneously distributed in the OM coating in individual particles.
453 This suggests that some of the OM in the coating has the potential to act as BrC (Jiang
454 et al., 2019; Laskin et al., 2015).

455 To understand how OM coating influence optical properties of sulfate-containing
456 particles, we make an assumption that OM coating is strongly absorbing (case 1),
457 moderately absorbing (case 2) or non-absorbing BrC (case 3) with a refractive index
458 of 1.65-0.03i, 1.65-0.003i, and 1.65 at 550 nm according to Feng et al. (2013). Based
459 on the size measurements shown in Figure 7d, we can calculate volume of sulfate and
460 OM within each particle. We input volume of each component and the corresponding
461 refractive index into the Mie code and then calculated optical properties of individual
462 sulfate-containing particles in the samples. Based on optical data statistic of 575
463 particles, Figure 8a show that if the OM coating is strongly absorbing BrC (referred to

464 case Abs1), the average absorption cross section (ACS) of individual particles is
465 estimated to be $2.67 \times 10^{-14} \text{ m}^2$. This value is 8.30 times higher than the aerosol ACS
466 ($3.22 \times 10^{-15} \text{ m}^2$) when assuming that the BrC is moderately absorbing (referred to case
467 Abs2, Figure 8a). However, the scattering cross section (SCS) of individual particles
468 only shows a small change (Figure 8b). Figure 8c also shows that the single scattering
469 albedos (SSAs) of individual particles are 0.92, 0.99, and 1 when assuming the OM as
470 strongly, moderately and non-absorbing BrC (cases SSA1 to SSA3). These results
471 suggest that whether we consider organic coating as BrC may have a significant
472 influence on the absorption properties of individual sulfate-containing particles.

473 In this study, we explored the relationship between ACS of individual particles
474 and particle diameters. Interestingly, Figure 8d shows that ACS of individual fine
475 OM-coating sulfate particles increased with particle size. This suggests that the ACS
476 of individual particles may increase as they grow and age in the atmosphere.

477 Current climate models estimated the radiative force of Arctic BC (Sand et al.,
478 2013; Shindell, 2007; Winiger et al., 2017; Zanatta et al., 2018), but none specifically
479 considered optical properties of Arctic BrC. Our study revealed the OM coating on
480 individual sulfate particles, which should be considered in aerosol radiation effect and
481 cloud-aerosol interaction simulations in the models.

482

483 **5 Summary**

484 A range of individual particle observation techniques, such as TEM/EDS, STEM,
485 SEM, NanoSIMS, and AFM, were applied to study S-rich, soot, and OM particles in
486 the Arctic atmosphere in the summer 2012. Sulfate-containing particles account for
487 approximately $29 \pm 7\%$ by number of all analysed particles. TEM and NanoSIMS
488 showed that individual sulfate-containing particles have OM coating with sulfate as
489 core. The SOM on the surfaces of fine particles may affect heterogeneous reactions
490 between reactive gases and sulfate particles in the Arctic air. Furthermore, 20% of the
491 sulfate-containing particles also contain small soot inclusions but they only appeared
492 in organic coating.

493 Size distribution of the secondary Arctic particles displayed a peak at 340 nm,

494 ranging from 100 nm to 2000 nm. The core particles, as sulfate or soot, had a peak at
495 240 nm and 120 nm, respectively. OM coating on average contribute $63 \pm 23\%$ by
496 volume to the dry NSS-particles. We also found that whether the OM coating may
497 have a significant influence on the absorption properties of individual particles in the
498 Arctic air, depending on the optical properties of the OM.
499

500 **Author Contributions:** WL and ZS designed the study. YZ and XS collected aerosol
501 particles. WL, HY, and JZ contributed laboratory experiments and data analysis. HY
502 and WL performed optical calculation and wrote part of first draft. PT and MD
503 provided the online measurement data of new particle formation and growth. JS and
504 XZ coordinated the field campaign. All authors commented and edited the paper.

505

506 **Competing interests:** The authors declare no competing financial interests

507

508 **Acknowledgments** We thank Boris Quennehen to provide data from the
509 FLEXPART-WRF. This work was funded by National Natural Science Foundation of
510 China (41622504, 41575116, 31700475) and the Hundred Talents Program in
511 Zhejiang University, Z.S. acknowledges funding from NERC (NE/S00579X/1).

References

- Abbatt, J.P.D., Leaitch, W.R., Aliabadi, A.A., Bertram, A.K., Blanchet, J.P., Boivin-Rioux, A., Bozem, H., Burkart, J., Chang, R.Y.W., Charette, J., Chaubey, J.P., Christensen, R.J., Cirisan, A., Collins, D.B., Croft, B., Dionne, J., Evans, G.J., Fletcher, C.G., Gal í M., Ghahremaninezhad, R., Girard, E., Gong, W., Gosselin, M., Gourdal, M., Hanna, S.J., Hayashida, H., Herber, A.B., Hesaraki, S., Hoor, P., Huang, L., Hussherr, R., Irish, V.E., Keita, S.A., Kodros, J.K., Köllner, F., Kolonjari, F., Kunkel, D., Ladino, L.A., Law, K., Levasseur, M., Libois, Q., Liggio, J., Lizotte, M., Macdonald, K.M., Mahmood, R., Martin, R.V., Mason, R.H., Miller, L.A., Moravek, A., Mortenson, E., Mungall, E.L., Murphy, J.G., Namazi, M., Norman, A.L., O'Neill, N.T., Pierce, J.R., Russell, L.M., Schneider, J., Schulz, H., Sharma, S., Si, M., Staebler, R.M., Steiner, N.S., Thomas, J.L., von Salzen, K., Wentzell, J.J.B., Willis, M.D., Wentworth, G.R., Xu, J.W., Yakobi-Hancock, J.D.: Overview paper: New insights into aerosol and climate in the Arctic, *Atmos. Chem. Phys.*, 19 (4), 2527-2560, 2019.
- Alexander, D.T.L., Crozier, P.A., Anderson, J.R.: Brown Carbon Spheres in East Asian Outflow and Their Optical Properties, *Science*, 321 (5890), 833-836, 2008.
- Andreae, M.O., Gelencser, A.: Black carbon or brown carbon? The nature of light-absorbing carbonaceous aerosols, *Atmos. Chem. Phys.*, 6 (10), 3131-3148, 2006.
- Behrenfeldt, U., Krejci, R., Ström, J., Stohl, A.: Chemical properties of Arctic aerosol particles collected at the Zeppelin station during the aerosol transition period in May and June of 2004, *Tellus B*, 60 (3), 405-415, 2008.
- Bohren, C.F., Huffman, D.R., 1983. Absorption and scattering of light by small particles. John Wiley & Sons, Inc. , New York, USA.
- Bond, T.C., Doherty, S.J., Fahey, D.W., Forster, P.M., Berntsen, T., DeAngelo, B.J., Flanner, M.G., Ghan, S., Kärcher, B., Koch, D., Kinne, S., Kondo, Y., Quinn, P.K., Sarofim, M.C., Schultz, M.G., Schulz, M., Venkataraman, C., Zhang, H., Zhang, S., Bellouin, N., Guttikunda, S.K., Hopke, P.K., Jacobson, M.Z., Kaiser, J.W., Klimont, Z., Lohmann, U., Schwarz, J.P., Shindell, D., Storelvmo, T., Warren, S.G., Zender, C.S.: Bounding the role of black carbon in the climate system: A scientific assessment, *J. Geophys. Res.*, 118 (11), 5380-5552, 2013.
- Brioude, J., Arnold, D., Stohl, A., Cassiani, M., Morton, D., Seibert, P., Angevine, W., Evan, S., Dingwell, A., Fast, J.D., Easter, R.C., Pisso, I., Burkhart, J., Wotawa, G.: The Lagrangian particle dispersion model FLEXPART-WRF version 3.1, *Geosci. Model Dev.*, 6 (6), 1889-1904, 2013.
- Brock, C.A., Cozic, J., Bahreini, R., Froyd, K.D., Middlebrook, A.M., McComiskey, A., Brioude, J., Cooper, O.R., Stohl, A., Aikin, K.C., de Gouw, J.A., Fahey, D.W., Ferrare, R.A., Gao, R.S., Gore, W., Holloway, J.S., Hübler, G., Jefferson, A., Lack, D.A., Lance, S., Moore, R.H., Murphy, D.M., Nenes, A., Novelli, P.C., Nowak, J.B., Ogren, J.A., Peischl, J., Pierce, R.B., Pilewskie, P., Quinn, P.K., Ryerson, T.B., Schmidt, K.S., Schwarz, J.P., Sodemann, H., Spackman, J.R., Stark, H., Thomson, D.S., Thornberry, T., Veres, P., Watts, L.A., Warneke, C., Wollny, A.G.: Characteristics, sources, and transport of aerosols measured in spring 2008 during the aerosol, radiation, and cloud processes affecting Arctic Climate (ARCPAC) Project, *Atmos. Chem. Phys.*, 11 (6), 2423-2453, 2011.
- Browse, J., Carslaw, K.S., Schmidt, A., Corbett, J.J.: Impact of future Arctic shipping on high-latitude black carbon deposition, *Geophys. Res. Lett.*, 40 (16), 4459-4463, 2013.
- Burkart, J., Willis, M.D., Bozem, H., Thomas, J.L., Law, K., Hoor, P., Aliabadi, A.A., Köllner, F., Schneider, J., Herber, A., Abbatt, J.P.D., Leaitch, W.R.: Summertime observations of elevated levels of ultrafine particles in the high Arctic marine boundary layer, *Atmos. Chem. Phys.*, 17 (8),

- 5515-5535, 2017.
- Buseck, P.R., Posfai, M.: Airborne minerals and related aerosol particles: Effects on climate and the environment, *P. Natl. Acad. Sci. USA*, 96 (7), 3372-3379, 1999.
- Chang, R.Y.W., Leck, C., Graus, M., Müller, M., Paatero, J., Burkhardt, J.F., Stohl, A., Orr, L.H., Hayden, K., Li, S.M., Hansel, A., Tjernström, M., Leaitch, W.R., Abbatt, J.P.D.: Aerosol composition and sources in the central Arctic Ocean during ASCOS, *Atmos. Chem. Phys.*, 11 (20), 10619-10636, 2011.
- Chi, J.W., Li, W.J., Zhang, D.Z., Zhang, J.C., Lin, Y.T., Shen, X.J., Sun, J.Y., Chen, J.M., Zhang, X.Y., Zhang, Y.M., Wang, W.X.: Sea salt aerosols as a reactive surface for inorganic and organic acidic gases in the Arctic troposphere, *Atmos. Chem. Phys.*, 15 (19), 11341-11353, 2015.
- Dagsson-Waldhauserova, P., Arnalds, O., Olafsson, H.: Long-term frequency and characteristics of dust storm events in Northeast Iceland (1949–2011), *Atmos. Environ.*, 77 (0), 117-127, 2013.
- Dall'Osto, M., Beddows, D.C.S., Tunved, P., Krejci, R., Ström, J., Hansson, H.C., Yoon, Y.J., Park, K.-T., Becagli, S., Udisti, R., Onasch, T., O'Dowd, C.D., Simó, R., Harrison, R.M.: Arctic sea ice melt leads to atmospheric new particle formation, *Sci. Rep.*, 7 (1), 3318, 2017.
- Doherty, S.J., Grenfell, T.C., Forsström, S., Hegg, D.L., Brandt, R.E., Warren, S.G.: Observed vertical redistribution of black carbon and other insoluble light-absorbing particles in melting snow, *J. Geophys. Res.*, 118 (11), 5553-5569, 2013.
- Feng, Y., Ramanathan, V., Kotamarthi, V.R.: Brown carbon: a significant atmospheric absorber of solar radiation?, *Atmos. Chem. Phys.*, 13 (17), 8607-8621, 2013.
- Fu, P., Kawamura, K., Barrie, L.A.: Photochemical and Other Sources of Organic Compounds in the Canadian High Arctic Aerosol Pollution during Winter–Spring, *Environ. Sci. Technol.*, 43 (2), 286-292, 2008.
- Geng, H., Ryu, J., Jung, H.-J., Chung, H., Ahn, K.-H., Ro, C.-U.: Single-Particle Characterization of Summertime Arctic Aerosols Collected at Ny-Alesund, Svalbard, *Environ. Sci. Technol.*, 44 (7), 2348-2353, 2010.
- Ghosal, S., Weber, P.K., Laskin, A.: Spatially resolved chemical imaging of individual atmospheric particles using nanoscale imaging mass spectrometry: insight into particle origin and chemistry, *Analytical Methods*, 6 (8), 2444-2451, 2014.
- Gilgen, A., Huang, W.T.K., Ickes, L., Neubauer, D., Lohmann, U.: How important are future marine and shipping aerosol emissions in a warming Arctic summer and autumn?, *Atmos. Chem. Phys.*, 18 (14), 10521-10555, 2018.
- Hansen, J., Nazarenko, L.: Soot climate forcing via snow and ice albedos, *P. Natl. Acad. Sci. USA*, 101 (2), 423-428, 2004.
- Hara, K., Yamagata, S., Yamanouchi, T., Sato, K., Herber, A., Iwasaka, Y., Nagatani, M., Nakata, H.: Mixing states of individual aerosol particles in spring Arctic troposphere during ASTAR 2000 campaign, *J. Geophys. Res.*, 108 (D7), 2003.
- Hegg, D.A., Warren, S.G., Grenfell, T.C., Sarah, J.D., Clarke, A.D.: Sources of light-absorbing aerosol in arctic snow and their seasonal variation, *Atmos. Chem. Phys.*, 10 (22), 10923-10938, 2010.
- Herrmann, A.M., Ritz, K., Nunan, N., Clode, P.L., Pett-Ridge, J., Kilburn, M.R., Murphy, D.V., O'Donnell, A.G., Stockdale, E.A.: Nano-scale secondary ion mass spectrometry — A new analytical tool in biogeochemistry and soil ecology: A review article, *Soil Biol. Biochem.*, 39 (8), 1835-1850, 2007.
- IPCC (2013), Clouds and Aerosols, in *Climate Change 2013: The Physical Science Basis. Contribution*

- of Working Group I to the Fifth Assessment Report of the Intergovernmental Panel on Climate Change, 571-657 pp, Cambridge, U.K. and New York, NY.
- Iwasaka, Y., Minoura, H., Nagaya, K.: The transport and spatial scale of Asian dust-storm clouds: A case study of the dust-storm event of April 1979, *Tellus, Ser. B*, 35, 189-196, 1983.
- Iziomon, M.G., Lohmann, U., Quinn, P.K.: Summertime pollution events in the Arctic and potential implications, *J. Geophys. Res.*, 111 (D12), D12206, 2006.
- Jacob, D.J., Crawford, J.H., Maring, H., Clarke, A.D., Dibb, J.E., Emmons, L.K., Ferrare, R.A., Hostetler, C.A., Russell, P.B., Singh, H.B., Thompson, A.M., Shaw, G.E., McCauley, E., Pederson, J.R., Fisher, J.A.: The Arctic Research of the Composition of the Troposphere from Aircraft and Satellites (ARCTAS) mission: design, execution, and first results, *Atmos. Chem. Phys.*, 10 (11), 5191-5212, 2010.
- Jiang, H., Frie, A.L., Lavi, A., Chen, J.Y., Zhang, H., Bahreini, R., Lin, Y.-H.: Brown Carbon Formation from Nighttime Chemistry of Unsaturated Heterocyclic Volatile Organic Compounds, *Environ. Sci. Techn. Lett.*, DOI: 10.1021/acs.estlett.1029b00017, 2019.
- Karl, M., Leck, C., Coz, E., Heintzenberg, J.: Marine nanogels as a source of atmospheric nanoparticles in the high Arctic, *Geophys. Res. Lett.*, 40 (14), 3738-3743, 2013.
- Kirpes, R.M., Bondy, A.L., Bonanno, D., Moffet, R.C., Wang, B., Laskin, A., Ault, A.P., Pratt, K.A.: Secondary sulfate is internally mixed with sea spray aerosol and organic aerosol in the winter Arctic, *Atmos. Chem. Phys.*, 18 (6), 3937-3949, 2018.
- Koch, D., Hansen, J.: Distant origins of Arctic black carbon: A Goddard Institute for Space Studies ModelE experiment, *J. Geophys. Res.*, 110 (D4), D04204, 2005.
- Lack, D.A., Langridge, J.M., Bahreini, R., Cappa, C.D., Middlebrook, A.M., Schwarz, J.P.: Brown carbon and internal mixing in biomass burning particles, *P. Natl. Acad. Sci. USA*, 109 (37), 14802-14807, 2012.
- Laskin, A., Laskin, J., Nizkorodov, S.A.: Chemistry of Atmospheric Brown Carbon, *Chem. Rev.*, 115 (10), 4355-4382, 2015.
- Laskina, O., Morris, H.S., Grandquist, J.R., Estillore, A.D., Stone, E.A., Grassian, V.H., Tivanski, A.V.: Substrate-Deposited Sea Spray Aerosol Particles: Influence of Analytical Method, Substrate, and Storage Conditions on Particle Size, Phase, and Morphology, *Environ. Sci. Tech.*, 49 (22), 13447-13453, 2015.
- Latham, T.L., Beyersdorf, A.J., Thornhill, K.L., Winstead, E.L., Cubison, M.J., Hecobian, A., Jimenez, J.L., Weber, R.J., Anderson, B.E., Nenes, A.: Analysis of CCN activity of Arctic aerosol and Canadian biomass burning during summer 2008, *Atmos. Chem. Phys.*, 13 (5), 2735-2756, 2013.
- Law, K.S., Stohl, A.: Arctic Air Pollution: Origins and Impacts, *Science*, 315 (5818), 1537-1540, 2007.
- Leck, C., Bigg, E.K.: Comparison of sources and nature of the tropical aerosol with the summer high Arctic aerosol, *Tellus, Ser. B*, 60 (1), 118-126, 2008.
- Leck, C., Svensson, E.: Importance of aerosol composition and mixing state for cloud droplet activation over the Arctic pack ice in summer, *Atmos. Chem. Phys.*, 15 (5), 2545-2568, 2015.
- Li, W., Sun, J., Xu, L., Shi, Z., Riemer, N., Sun, Y., Fu, P., Zhang, J., Lin, Y., Wang, X., Shao, L., Chen, J., Zhang, X., Wang, Z., Wang, W.: A conceptual framework for mixing structures in individual aerosol particles, *J. Geophys. Res.*, 121 (22), 13784-713,798, 2016.
- Li, W., Xu, L., Liu, X., Zhang, J., Lin, Y., Yao, X., Gao, H., Zhang, D., Chen, J., Wang, W., Harrison, R.M., Zhang, X., Shao, L., Fu, P., Nenes, A., Shi, Z.: Air pollution-aerosol interactions produce more bioavailable iron for ocean ecosystems, *Sci. Adv.*, 3 (3), e1601749, 2017.

- Maahn, M., de Boer, G., Creamean, J.M., Feingold, G., McFarquhar, G.M., Wu, W., Mei, F.: The observed influence of local anthropogenic pollution on northern Alaskan cloud properties, *Atmos. Chem. Phys.*, 17 (23), 14709-14726, 2017.
- Martin, M., Chang, R.Y.W., Sierau, B., Sjogren, S., Swietlicki, E., Abbatt, J.P.D., Leck, C., Lohmann, U.: Cloud condensation nuclei closure study on summer arctic aerosol, *Atmos. Chem. Phys.*, 11 (22), 11335-11350, 2011.
- Moffet, R.C., Rödel, T.C., Kelly, S.T., Yu, X.Y., Carroll, G.T., Fast, J., Zaveri, R.A., Laskin, A., Gilles, M.K.: Spectro-microscopic measurements of carbonaceous aerosol aging in Central California, *Atmos. Chem. Phys.*, 13 (20), 10445-10459, 2013.
- Moore, R.H., Bahreini, R., Brock, C.A., Froyd, K.D., Cozic, J., Holloway, J.S., Middlebrook, A.M., Murphy, D.M., Nenes, A.: Hygroscopicity and composition of Alaskan Arctic CCN during April 2008, *Atmos. Chem. Phys.*, 11 (22), 11807-11825, 2011.
- Moroni, B., Cappelletti, D., Crocchianti, S., Becagli, S., Caiazzo, L., Traversi, R., Udusti, R., Mazzola, M., Markowicz, K., Ritter, C., Zielinski, T.: Morphochemical characteristics and mixing state of long range transported wildfire particles at Ny-Ålesund (Svalbard Islands), *Atmos. Environ.*, 156, 135-145, 2017.
- Park, K., Kim, G., Kim, J.-s., Yoon, Y.-J., Cho, H.-j., Ström, J.: Mixing State of Size-Selected Submicrometer Particles in the Arctic in May and September 2012, *Environ. Sci. Technol.*, 48 (2), 909-919, 2013.
- Peters, G.P., Nilssen, T.B., Lindholt, L., Eide, M.S., Glomsrød, S., Eide, L.I., Fuglestad, J.S.: Future emissions from shipping and petroleum activities in the Arctic, *Atmos. Chem. Phys.*, 11 (11), 5305-5320, 2011.
- Qi, L., Li, Q., Li, Y., He, C.: Factors controlling black carbon distribution in the Arctic, *Atmos. Chem. Phys.*, 17 (2), 1037-1059, 2017.
- Quinn, P.K., Shaw, G., Andrews, E., Dutton, E.G., Ruoho-Airola, T., Gong, S.L.: Arctic haze: current trends and knowledge gaps, *Tellus B*, 59 (1), 99-114, 2007.
- Raatikainen, T., Brus, D., Hyvärinen, A.P., Svensson, J., Asmi, E., Lihavainen, H.: Black carbon concentrations and mixing state in the Finnish Arctic, *Atmos. Chem. Phys.*, 15 (17), 10057-10070, 2015.
- Riemer, N., West, M., Zaveri, R.A., Easter, R.C.: Simulating the evolution of soot mixing state with a particle resolved aerosol model, *J. Geophys. Res.*, 114, doi:10.1029/2008JD011073, 2009.
- Riemer, N., Ault, A.P., West, M., Craig, R.L., Curtis, J.H.: Aerosol Mixing State: Measurements, Modeling, and Impacts, *Rev. Geophys.*, 57, <https://doi.org/10.1029/2018RG000615>, 2019.
- Saleh, R., Hennigan, C.J., McMeeking, G.R., Chuang, W.K., Robinson, E.S., Coe, H., Donahue, N.M., Robinson, A.L.: Absorptivity of brown carbon in fresh and photo-chemically aged biomass-burning emissions, *Atmos. Chem. Phys.*, 13 (15), 7683-7693, 2013.
- Samset, B.H., Myhre, G., Herber, A., Kondo, Y., Li, S.M., Moteki, N., Koike, M., Oshima, N., Schwarz, J.P., Balkanski, Y., Bauer, S.E., Bellouin, N., Berntsen, T.K., Bian, H., Chin, M., Diehl, T., Easter, R.C., Ghan, S.J., Iversen, T., Kirkevåg, A., Lamarque, J.F., Lin, G., Liu, X., Penner, J.E., Schulz, M., Seland, Ø., Skeie, R.B., Stier, P., Takemura, T., Tsigaridis, K., Zhang, K.: Modelled black carbon radiative forcing and atmospheric lifetime in AeroCom Phase II constrained by aircraft observations, *Atmos. Chem. Phys.*, 14 (22), 12465-12477, 2014.
- Sand, M., Berntsen, T.K., Kay, J.E., Lamarque, J.F., Seland, Ø., Kirkevåg, A.: The Arctic response to remote and local forcing of black carbon, *Atmos. Chem. Phys.*, 13 (1), 211-224, 2013.

- Seinfeld, J., Pandis, S., 2006. *Atmospheric Chemistry and Physics: From air pollution to climate change* (2nd ed.). 1-1203 pp., John Wiley & Son, Inc., Hoboken, New Jersey.
- Shindell, D.: Local and remote contributions to Arctic warming, *Geophys. Res. Lett.*, 34 (14), L14704, 2007.
- Sierau, B., Chang, R.Y.W., Leck, C., Paatero, J., Lohmann, U.: Single-particle characterization of the high-Arctic summertime aerosol, *Atmos. Chem. Phys.*, 14 (14), 7409-7430, 2014.
- Tobo, Y., Adachi, K., DeMott, P.J., Hill, T.C.J., Hamilton, D.S., Mahowald, N.M., Nagatsuka, N., Ohata, S., Uetake, J., Kondo, Y., Koike, M.: Glacially sourced dust as a potentially significant source of ice nucleating particles, *Nature Geoscience*, 12 (4), 253-258, 2019.
- Updyke, K.M., Nguyen, T.B., Nizkorodov, S.A.: Formation of brown carbon via reactions of ammonia with secondary organic aerosols from biogenic and anthropogenic precursors, *Atmos. Environ.*, 63 (0), 22-31, 2012.
- Wärnschimmel, H., MacLeod, M., Hungerbühler, K.: Emissions, Fate and Transport of Persistent Organic Pollutants to the Arctic in a Changing Global Climate, *Environ. Sci. Technol.*, 47 (5), 2323-2330, 2013.
- Wang, B., Laskin, A., Roedel, T., Gilles, M.K., Moffet, R.C., Tivanski, A.V., Knopf, D.A.: Heterogeneous ice nucleation and water uptake by field-collected atmospheric particles below 273 K, *J. Geophys. Res.*, 117, 2012.
- Wang, X., Heald, C.L., Liu, J., Weber, R.J., Campuzano-Jost, P., Jimenez, J.L., Schwarz, J.P., Perring, A.E.: Exploring the observational constraints on the simulation of brown carbon, *Atmos. Chem. Phys.*, 18 (2), 635-653, 2018.
- Wang, Z., Bi, L., Yi, B., Zhang, X.: How the Inhomogeneity of Wet Sea Salt Aerosols Affects Direct Radiative Forcing, *Geophysical Research Letters*, 46 (3), 1805-1813, 2019.
- Weinbruch, S., Wiesemann, D., Ebert, M., Schütze, K., Kallenborn, R., Ström, J.: Chemical composition and sources of aerosol particles at Zeppelin Mountain (Ny Ålesund, Svalbard): An electron microscopy study, *Atmos. Environ.*, 49 (0), 142-150, 2012.
- Winiger, P., Andersson, A., Eckhardt, S., Stohl, A., Gustafsson, Ö.: The sources of atmospheric black carbon at a European gateway to the Arctic, *Nat. Commun.*, 7, 12776, 2016.
- Winiger, P., Andersson, A., Eckhardt, S., Stohl, A., Semiletov, I.P., Dudarev, O.V., Charkin, A., Shakhova, N., Klimont, Z., Heyes, C., Gustafsson, Ö.: Siberian Arctic black carbon sources constrained by model and observation, *P. Natl. Acad. Sci. USA*, 114 (7), E1054-E1061, 2017.
- Xu, J.W., Martin, R.V., Morrow, A., Sharma, S., Huang, L., Leaitch, W.R., Burkart, J., Schulz, H., Zanutta, M., Willis, M.D., Henze, D.K., Lee, C.J., Herber, A.B., Abbatt, J.P.D.: Source attribution of Arctic black carbon constrained by aircraft and surface measurements, *Atmos. Chem. Phys.*, 17 (19), 11971-11989, 2017.
- Yang, Y., Wang, H., Smith, S.J., Easter, R.C., Rasch, P.J.: Sulfate Aerosol in the Arctic: Source Attribution and Radiative Forcing, *J. Geophys. Res.*, 123 (3), 1899-1918, 2018.
- You, Y., Renbaum-Wolff, L., Carreras-Sospedra, M., Hanna, S.J., Hiranuma, N., Kamal, S., Smith, M.L., Zhang, X., Weber, R.J., Shilling, J.E., Dabdub, D., Martin, S.T., Bertram, A.K.: Images reveal that atmospheric particles can undergo liquid-liquid phase separations, *P. Natl. Acad. Sci. USA*, 109 (33), 13188-13193, 2012.
- Zanutta, M., Laj, P., Gysel, M., Baltensperger, U., Vratolis, S., Eleftheriadis, K., Kondo, Y., Dubuisson, P., Winiarek, V., Kazadzis, S., Tunved, P., Jacobi, H.W.: Effects of mixing state on optical and radiative properties of black carbon in the European Arctic, *Atmos. Chem. Phys.*, 18 (19),

14037-14057, 2018.

Zangrando, R., Barbaro, E., Zennaro, P., Rossi, S., Kehrwald, N.M., Gabrieli, J., Barbante, C., Gambaro, A.: Molecular Markers of Biomass Burning in Arctic Aerosols, *Environ. Sci. Technol.*, 47 (15), 8565-8574, 2013.

Figure Captions

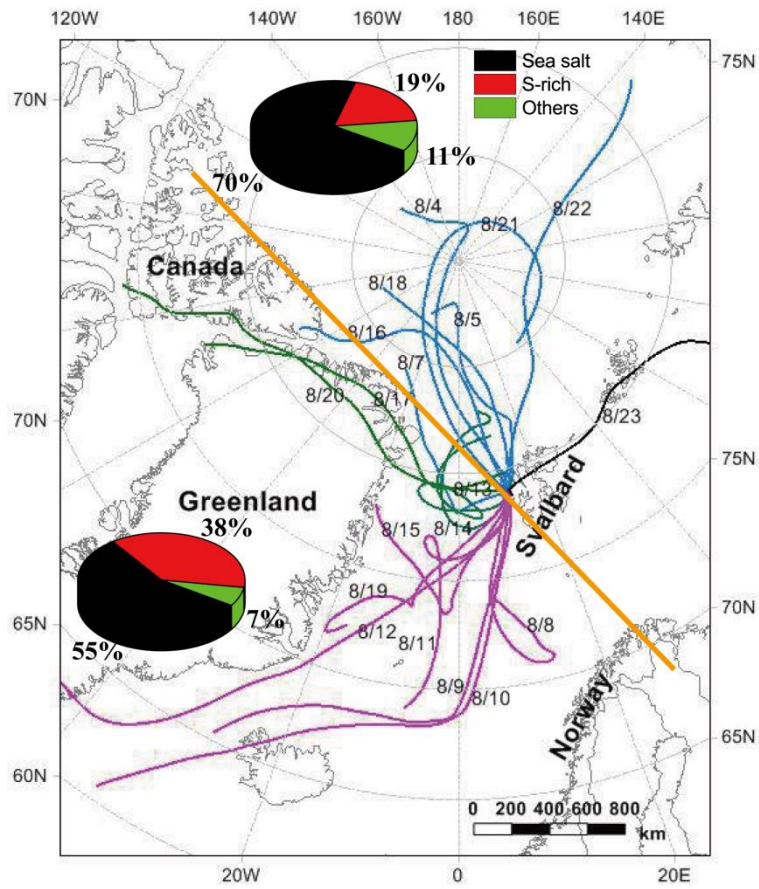


Figure 1 72 h back trajectories of air masses at 500 m over Arctic Yellow River Station in Svalbard during 3–26 August 2012, and arriving time was set according to the sampling time. Air masses were divided into two groups by the yellow line: one group from the central Arctic Ocean and the other one from North America and Greenland. Pie charts show the number fractions of sea salt, S-rich, and other particles.

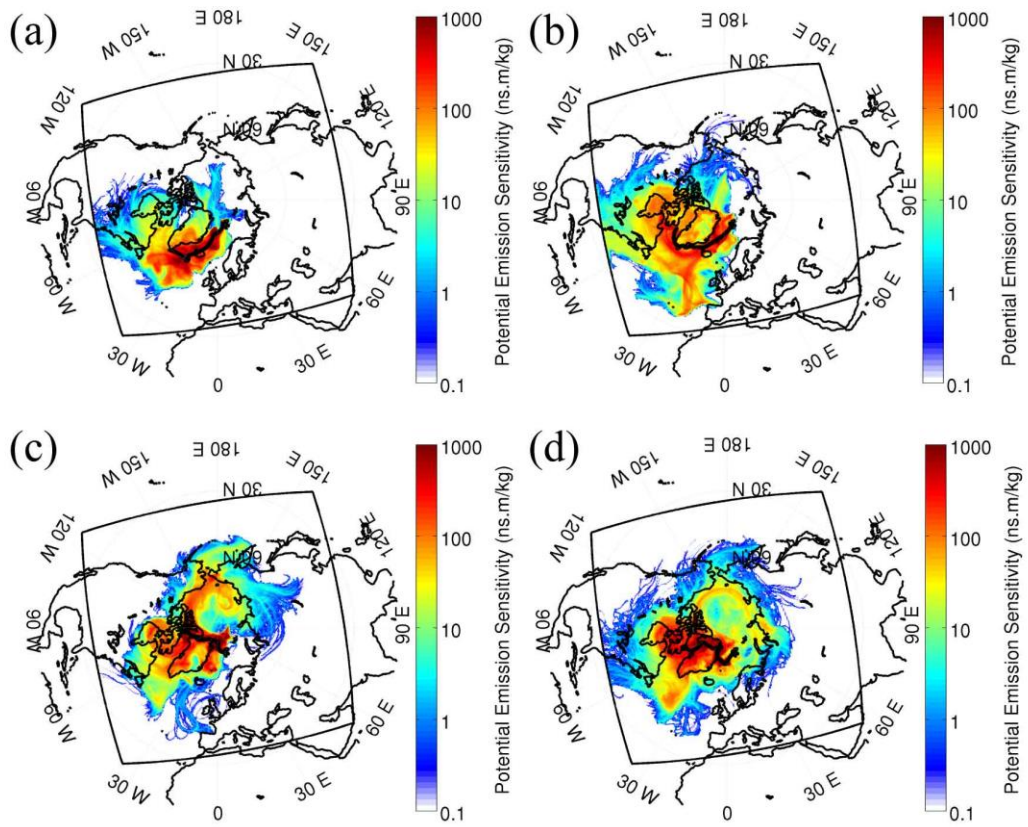


Figure 2 FLEXPART-WRF on August 11, 12, 14, and 15, 2012. Black square shows the WRF domain used to initiate the FLEXPART-WRF simulation.

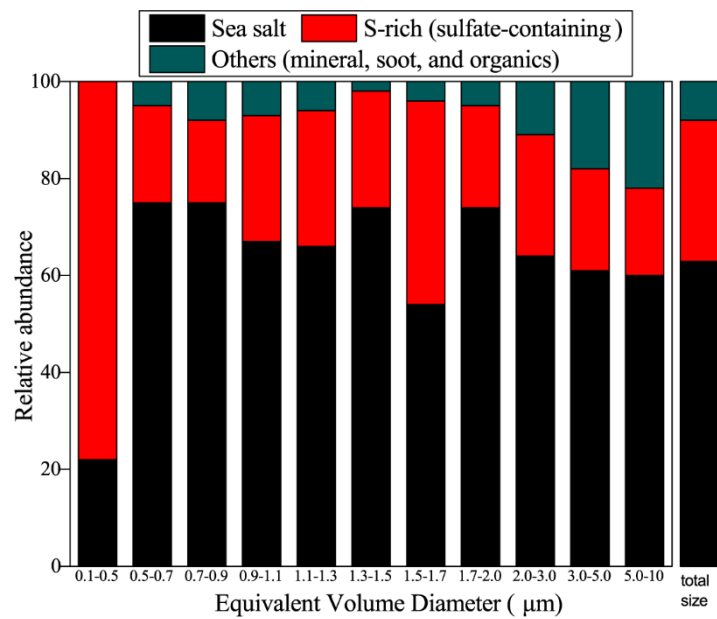


Figure 3 Relative abundances of typical individual aerosol particles in the analysed samples. Sulfate-containing particles include all particles that are internal mixture of sulfate and OM, with or without soot.

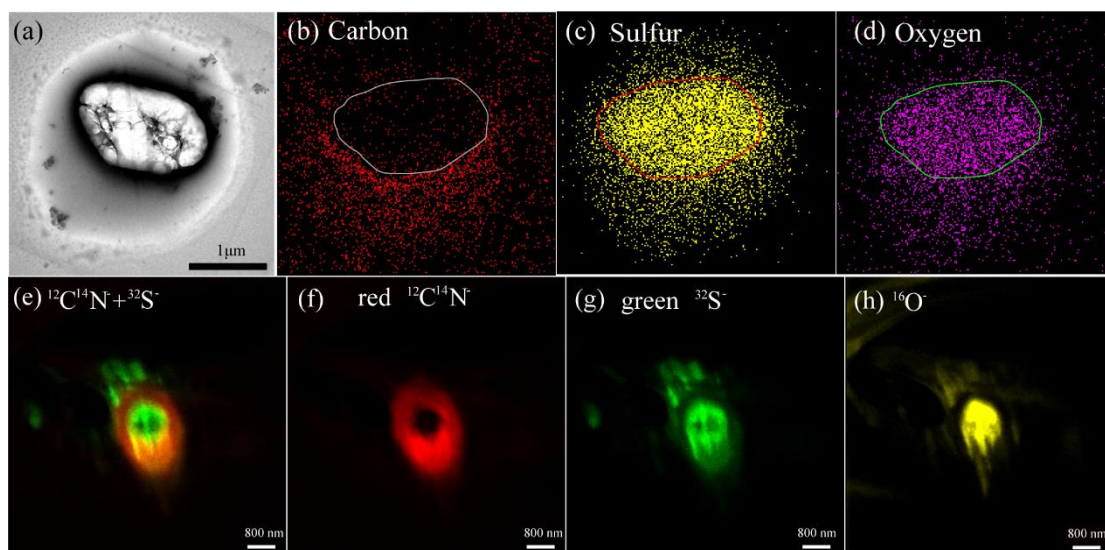


Figure 4 TEM images of a secondary particle and NanoSIMS intensity threshold maps of an aerosol particle with sulfate core and OM coating. (a) Bright-field TEM image of an internally mixed particle; (b) elemental carbon (c) sulfur and (d) oxygen maps of the internally mixed particle shown in 1(a); (e) Overlay of $^{12}\text{C}^{14}\text{N}^-$ and $^{32}\text{S}^-$ ion maps in an internally mixed particle; (f) CN^- map (g) S^- (h) O^- secondary ion maps. Ion maps with a set of aerosol particles were shown in Figure S1.

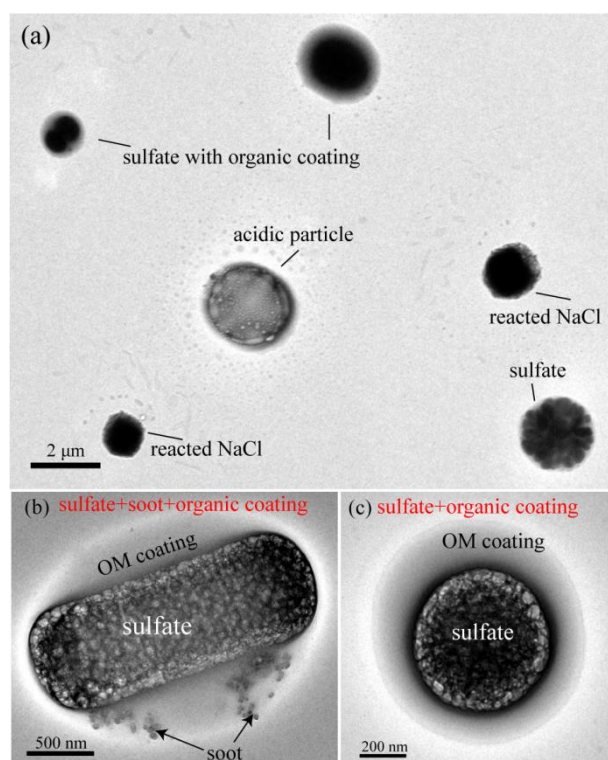


Figure 5 TEM images of individual particles containing sulfate, OM, and soot. (a) Low magnification TEM image showing sulfates, sulfate with OM coating, and reacted NaCl particles. (b) an internally mixed particle of sulfate and soot with OM coating (c) a particle with sulfate core and OM coating.

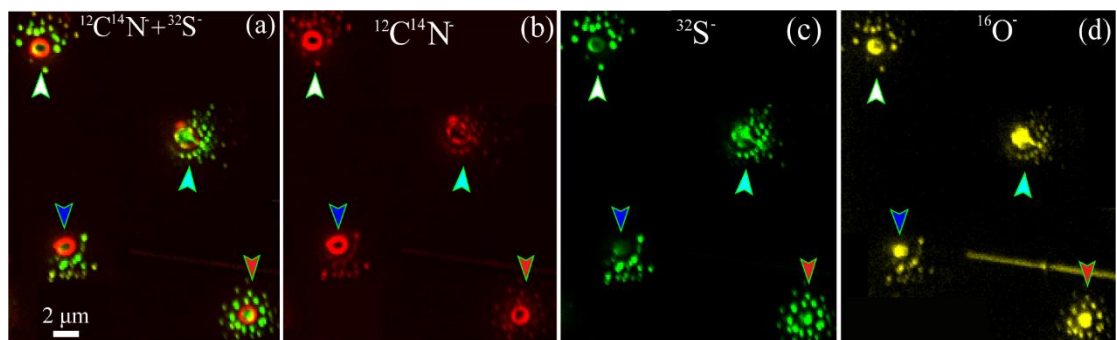


Figure 6 NanoSIMS intensity threshold maps of individual aerosol particles surrounded by satellite particles. (e) Overlay of $^{12}\text{C}^{14}\text{N}^-$ and $^{32}\text{S}^-$ ion maps of individual particles. (f) CN^- (g) S^- (h) O^- maps. Four particles were indicated by white, pink, blue, and red arrows.

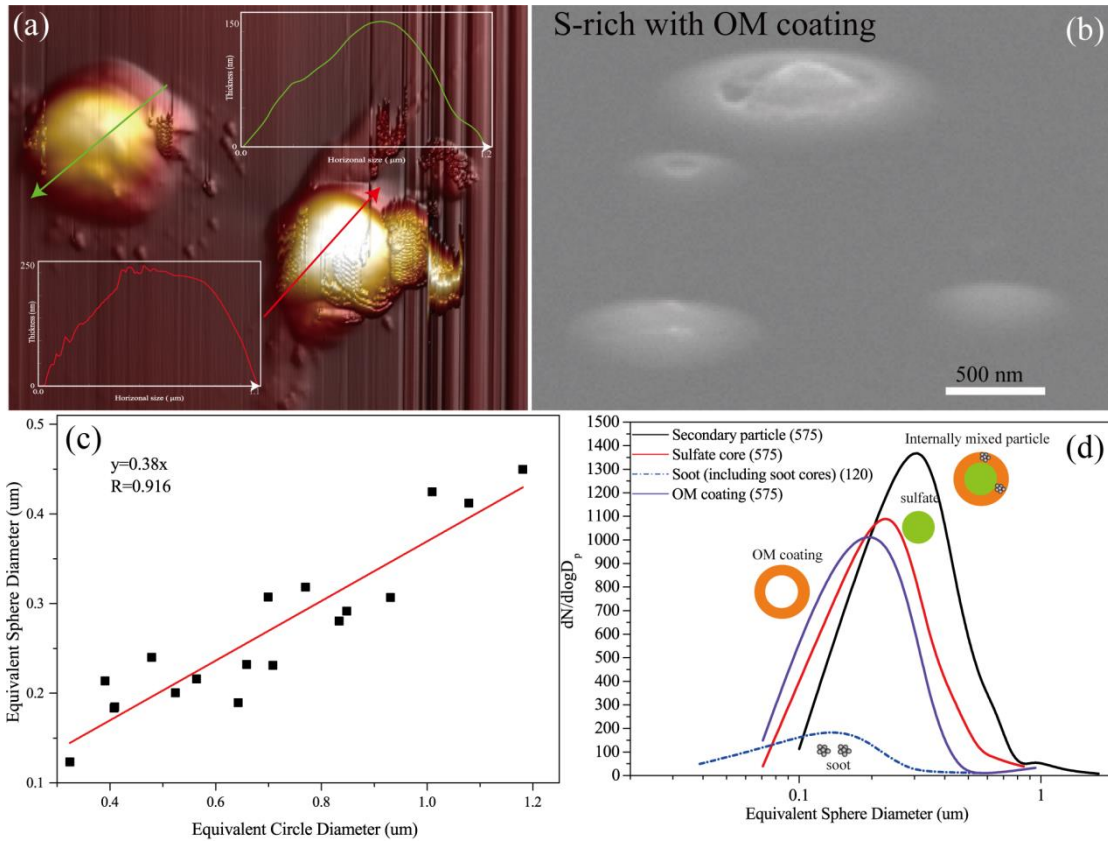


Figure 7 AFM image and calculated diameter of individual particles. (a) 3-D AFM image of sulfate-containing particles. The colored arrows represent the cross sections where the particles heights are measured (see insert figures). (b) SEM image of S-rich particles with OM coating obtained from 75° tilt of the SEM specimen stage (c) The near linear relationships between ECD and ESD based on S-rich particles with OM coating by atomic force microscopy. (d) Size distribution of individual particle with OM coating and sulfate core based on the estimated ESD diameter from TEM image.

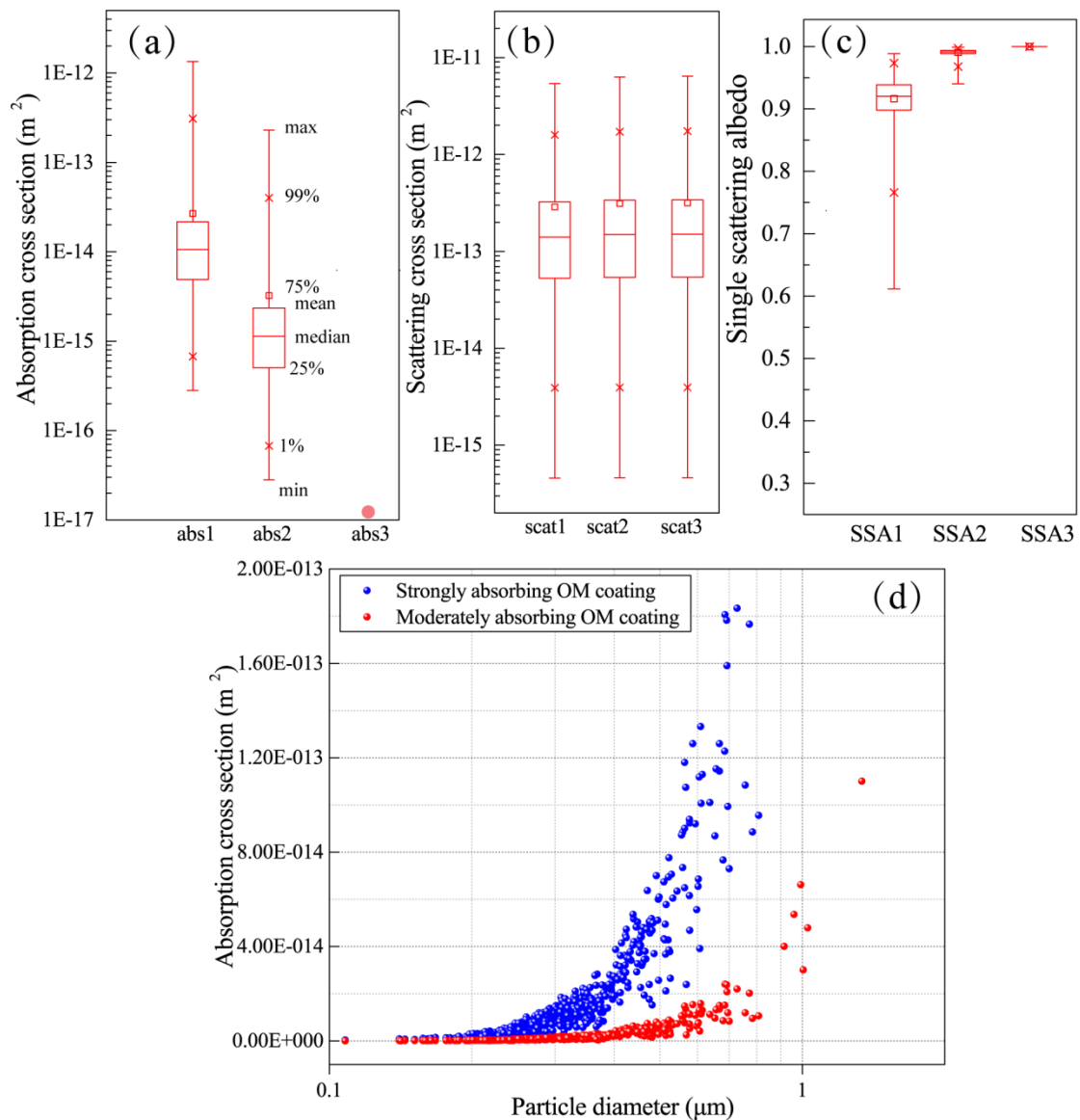


Figure 8 Optical properties of box-and-whisker plots showing optical parameters of all analysed particles assuming sulfate core and BrC shell (not considering soot cores in the particles). (a) Scattering cross section (b) Absorption cross section (c) Single scattering albedo. Top to bottom makers in the box-and-whisker represent max, 99%, 75%, mean, median, 25%, 1%, min values. (d) Absorption cross section along with particle diameter assuming strongly absorbing BrC and Moderate absorbing BrC as the particle OM coating. Abs 1, abs 2 and abs3 represent the BrC with highly, moderately and weak absorbing property.

Table 1 Sampling information in Arctic area and their analysis

Date	Local time	T	RH	P	WD	WS	TEM	EDS	SEM	AFM	NanoSIMS
2012.8.7	20:50 -21:15	4.9	84	1009.0	296	4.1	43	10			
2012.8.8	08:23 -08:48	4.9	81	1007.6	238	2.1	38	11			
2012.8.9	14:40 -15:05	6.6	81	1003.9	129	6.5	146	50			12
	15:20 -15:49	7.0	78	1003.5	120	7.3	130	26	20		
2012.8.10	00:15 -00:40	7.3	80	998.6	135	8.9	121	23			
2012.8.11	09:10 -09:35	6.2	94	997.0	303	3.3	128	50			10
2012.8.11	16:00 -16:25	4.1	92	1002.0	327	4.6	156	55		6	
2012.8.12	15:25 -15:50	5.7	83	1006.8	132	6.9	100	15	32		
2012.8.13	08:55 -09:20	5.3	81	1009.6	91	1.1	113	16			
2012.8.13	14:15 -14:40	4.5	90	1011.4	351	2.1	136	56			10
2012.8.14	09:50 -10:20	5.0	85	1019.7	351	2.3	134	24			
2012.8.14	15:12 -15:42	4.6	88	1020.5	117	2.6	121	26			
2012.8.14	21:17 -21:47	4.8	84	1020.7	276	5.4	178	56		5	
2012.8.15	09:15 -09:45	5.8	73	1019.6	135	3.7	165	60		6	
2012.8.15	15:00 -15:33	6.8	70	1018.9	270	3.3	80	11			
2012.8.17	9:00 -10:00	3.8	86	1017.1	116	0.3	30	15			
2012.8.17	14:50 -15:20	3.7	85	1015.7	109	2.2	42	16			
2012.8.21	15:05 -15:40	1.6	87	1003.7	314	6.8	46	18			
2012.8.22	08:55 -09:30	2.8	78	999.2	331	2.8	49	19			
2012.8.23	09:00 -09:40	3.4	64	998.0	136	6.9	21	9			
2012.8.23	20:35 -21:08	3.8	59	1002.0	138	6.3	25	9			

